Research Article | Vol. 31, No. 5 / 27 Feb 2023 / Optics Express 7599

Optics EXPRESS

Method for retrieving range-resolved aerosol microphysical properties from polarization lidar measurements

ZHONGWEI HUANG,[1,*] QINGQING DONG,[1] BIN CHEN,[1] TIANHE WANG,[1] JIANRONG BI,[1] TIAN ZHOU,[1] KHAN ALAM,[2] JINSEN SHI,[1] AND SHUANG ZHANG[1]

[1]*Collaborative Innovation Center for West Ecological Safety (CIWES), Lanzhou University, Lanzhou 730000, China*
[2]*Department of Physics, University of Peshawar, Peshawar 25120, KPK, Pakistan*
[*]*huangzhongwei@lzu.edu.cn*

Abstract: Aerosol microphysical properties, such as volume concentration (VC) and effective radius (ER), are of great importance to evaluate their radiative forcing and impacts on climate change. However, range-resolved aerosol VC and ER still cannot be obtained by remote sensing currently except for the column-integrated one from sun-photometer observation. In this study, a retrieval method of range-resolved aerosol VC and ER is firstly proposed based on the partial least squares regression (PLSR) and deep neural networks (DNN), combining polarization lidar and collocated AERONET (AErosol RObotic NETwork) sun-photometer observations. The results show that the measurement of widely-used polarization lidar can be reasonably used to derive the aerosol VC and ER, with the determination coefficient (R^2) of 0.89 (0.77) for VC (ER) by use of the DNN method. Moreover, it is proven that the lidar-based height-resolved VC and ER at near-surface are well consistent with independent observations of collocated Aerodynamic Particle Sizer (APS). Additionally, we found that there are significant diurnal and seasonal variations of aerosol VC and ER in the atmosphere at Semi-Arid Climate and Environment Observatory of Lanzhou University (SACOL). Compared with columnar ones from the sun-photometer observation, this study provides a reliable and practical way to obtain full-day range-resolved aerosol VC and ER from widely-used polarization lidar observation, even under cloud conditions. Moreover, this study also can be applied to long-term observations by current ground-based lidar networks and spaceborne CALIPSO lidar, aiming to further evaluate aerosol climatic effects more accurately.

1. Introduction

Atmosphere aerosols play an important role in the global climate and ecological environment, but there are still significant uncertainties because of the complexity of aerosols [1]. Aerosols not only absorb and scatter solar radiation to directly change the earth-atmosphere radiation balance but also indirectly affect the formation process of clouds and their microphysical properties [2–7]. To accurately evaluate their effects on climate and the environment, quantitative information on aerosol physical and chemical characterizations is needed [8–11].

Lidar, as an active remote sensing, has been widely used over the past decades [12–14]. It has unique advantages of aerosol detection with high spatiotemporal resolution, especially in the vertical direction [15]. Numerous studies have characterized atmospheric aerosols based on ground-based or spaceborne lidar measurements [16–19]. The combination of the depolarization ratio and extinction coefficient profiles measured by Raman lidar can distinguish biomass burning aerosols and mineral dust. Hair et al. found that the radiation effect of biomass burning aerosols is sensitive to the vertical distribution of aerosols by combining lidar observations and model

#481252 https://doi.org/10.1364/OE.481252
Journal © 2023 Received 17 Nov 2022; revised 30 Jan 2023; accepted 31 Jan 2023; published 15 Feb 2023

Optics EXPRESS

simulations [20]. By establishing a network, ground-based lidar can obtain large spatial scale and continuous four-dimensional atmospheric data to meet the needs of environmental, meteorological and climatic research [21]. AD-Net is a lidar network for the continuous observation of the vertical distribution of dust and other aerosols in East Asia [22]. Other lidar networks, such as the NASA Micro-Pulse Lidar Network (MPLNET) [23], the European Aerosol Research Lidar Network (EARLINET) [24,25] and the Network Detection of Atmospheric Composition Change (NDACC) [26] provide very important observational data for studying aerosol-cloud interaction at a large scale. Spaceborne lidar systems have a wider range of observations than ground-based lidar systems. The seasonal variation and the vertical distribution of aerosol can be observed by Cloud-Aerosol Lidar and Infrared Pathfinder Satellite Observation (CALIPSO) lidar measurements [27]. Yu et al. compared satellite-based lidar observation with the results of the Goddard Chemistry Aerosol Radiation Transport (GOCART) model simulations [28]. Vermier et al. found that there is an aerosol layer on the top of the troposphere in Asia during the Asian monsoon based on CALIPSO observations [29]. The aerosols vertical distribution characteristics have quantified by combining ground-based lidar and spaceborne lidar observations. The phenomenon of cross-border transport of urban aerosols in a large-area during haze events was found employing a combination of ground-based lidar and CALIPSO lidar measurements [30]. It is found that dust aerosols originating from the Taklimakan Desert can be lifted up to a height of 9 km and can be transported to the Western Pacific Ocean by long-range airmasses [31].

The optical and physical parameters of aerosols, such as the VC and ER of the particle, are important parameters to study the influence of aerosols on atmospheric processes, which are also necessary to characterize aerosol types [32,33]. Sun-photometer is a very effective tool to measure aerosol microphysical properties and has been widely used to study aerosol physical and optical properties of pollution events such as haze [34–36]. With the development of laser technology, lidar has been applied to the study of aerosol microphysical properties [37–40]. The aerosol size distribution can be derived from two-wavelength rotational Raman lidar observations [41]. Multi-wavelength Raman lidar observations of the scattering and absorption characteristics of different aerosols are usually used to further retrieve the microphysical characteristics of aerosols. A scanning Raman aerosol lidar system with 6 wavelength lasers and 11 channels receiving signals was first developed by Althausen et al. [42]. Then, the particle size distribution was obtained mainly by use of regularization technology and cross-validated with an error of approximately 20% [43]. Moreover, some important microphysical parameters of particles, such as the ER and number concentration, were inversed using only two extinction coefficients and three backscatter lidar systems ($3\beta + 2\alpha$) and were improved using an inversion method of ($3\beta + 2\alpha + 1\delta$) detected by a multi-wavelength Mie-Raman lidar system [44]. In addition, aerosol microphysical properties retrieved from satellite multi-wavelength lidar observations were simulated, and the inversion results were found to be acceptable based on only one extinction coefficient and three backscattering coefficients ($3\beta + 1\alpha$) [45]. However, there are still limitations for multi-wavelength lidar observations due to their high cost and complicated configuration as well as difficult maintenance.

The purpose of this paper is to study a simple and reliable way to derive the range-resolved VC and ER of aerosols from measurements observed by widely used lidar systems (such as Mie polarization lidar systems), which is based on partial least squares regression (PLSR) and deep neural networks (DNN). In this study, we use continuous polarization lidar measurements at Semi-Arid Climate and Environment Observatory of Lanzhou University (SACOL) (35.95°N, 104.14°E) over Northwest China and Osaka (34.65°N, 135.59°E) in Japan. The VC and ER of aerosols are derived from lidar measurements and validated by collocated AERONET and APS observations. Furthermore, seasonal variations of the range-resolved VC and ER are also investigated. Section 2 briefly introduces the instruments and observational data used in this

Optics EXPRESS

study. The retrieval method and validation are described in Section 3. Results and discussion are given in Section 4.

2. Instruments and observational data

2.1. Ground-based Mie polarization lidar system

The ground-based polarization lidar system used in this study was developed by the National Institute for Environmental Studies (NIES) of Japan for continuous network observations [22]. A flash-lamp-pumped Nd:YAG laser was employed to generate first- and second-harmonic outputs at wavelengths of 532 nm and 1064 nm. The energy of a single pulse is ~ 20 mJ, and the pulse repetition rate is 10 Hz. Then, backscattering signals from the atmosphere were collected by a receiver telescope with a diameter of 200 mm. The field of view (FOV) of the system is 1 mrad. The spatial resolution and temporal resolution of the lidar system are 6 m and 15 min, respectively. Polarization measurements were observed at 532 nm using polarizing beamsplitters (PBSs) and calibrated on site using a half-wave plate [46]. The depolarization ratio (DR) at 532 nm is defined as the ratio of the parallel to the perpendicular components of the backscattering signals, and the color ratio (CR) is defined as the ratio of the backscattering signals at 1064 nm to those at 532 nm. The vertical structure of tropospheric aerosols and clouds measured by the ground-based polarization lidar system at SACOL (from October 2009 to March 2011), Osaka (2013 and 2015) was used in this study. Compared with co-located AERONET results, profiles of lidar data were selected according to the time of sun-photometer observation. There is an uncertainty when converting volume DR to particle DR for Mie polarization lidar measurements. So, it is noted that volume DR is directly used in this paper.

2.2. AERONET sun-photometer

The AERONET sun-photometer is an automatic direct solar and sky radiometer that observes wavelengths of 440, 670, 870, and 1020 nm with spectral interference filters (10 nm bandwidth) for aerosol measurements [47–49]. Direct sun measurements are performed at these wavelengths to determine the aerosol optical depth (AOD). The water vapor content is retrieved using received signals at 940 nm. The instrument is calibrated annually by comparison with an AERONET master sun-photometer. The uncertainty of AOD retrieval is less than 0.02 for AERONET observations [50]. In this study, the VC and effective radius (ER) from the level 2.0 products of the collocated AERONET sun-photometer observations at SACOL and Osaka sites were also used. The calculation formulas are as follows,

$$VC = \int_{r\,\min}^{r\,\max} \frac{dV(r)}{d\ln r} d\ln r \tag{1}$$

$$ER = \frac{\int_{r\,\min}^{r\,\max} r^3 \frac{dN(r)}{d\ln r} d\ln r}{\int_{r\,\min}^{r\,\max} r^2 \frac{dN(r)}{d\ln r} d\ln r} \tag{2}$$

where dV(r)/dlnr ($\mu m^3/\mu m^2$) is aerosol size distribution of the particle volume, and dN(r)/dlnr is the distribution of the particle number.

2.3. Aerodynamic particle sizer (APS)

The APS 3321 (TSI, Inc., St. Paul, MN) is an instrument for measuring aerosol particle size distribution in the atmosphere [51]. Based on the principle of double laser particle size

Optics EXPRESS

measurement, the particle size distribution of aerosol particles can be determined by measuring the flight speed and flight time of particles between two laser beams. A particle size range of 0.5-20 µm can be measured [52,53]. The APS is suitable for field measurements because of its small size, simple operation and convenience. It can be used in environmental air monitoring, indoor air quality monitoring and so on [54,55]. In this study, APS observations at SACOL in 2010 were used to validate lidar-derived range-resolved VC and ER at near-surface.

3. Retrieval method and validation

As an active remote sensing tool, lidar has great advantages in continuous and range-resolved aerosol observation. There is a certain relationship between the lidar observations, and the aerosol microphysical characteristics observed by the sun-photometer. Figure 1 shows the lidar measurements and sun-photometer observations for two typical weather conditions at SACOL on February 4, 2010 and November 9, 2010. Figure 1(a) represents the attenuated backscattering coefficient (ABC) (532 nm), linear DR (532 nm) and CR (1064/532 nm) observed by the ground-based lidar system, showing the vertical structure of atmospheric aerosols. The aerosol VC, ER, and AOD observed by the collocated AERONET sun-photometer are shown in Fig. 1(b). On February 4, from the ground to approximately 1 km, the ABC has a strong backscatter signal greater than 0.01 (/sr/km), which indicates a dense dust layer loading. The linear DR is approximately 0.15 ~ 0.20 due to the non-spherical shape of dust particles, which can be used to characterize the shape of aerosol particles. A larger DR value of approximately 0.17 was also reported by previous study [56]. Additionally, the size of dust particles can also be characterized by the CR from lidar observations. Lidar signal intensity decreased from the ground to approximately 1 km at first and then increased on November 9, 2010. According to the variation of DR and CR, there was a mixed layer of dust and pollution. Overall, we can see that the variations of aerosol VC and ER are consistent with lidar results, which indicates that there is a certain correlation between these two observations.

Figure 2 shows the relationships between the DR and CR from lidar measurements and the VC and ER from AERONET sun-photometer observation at SACOL from October 2009 to March 2011 and Osaka sites from 2013 to 2015. Columnar DR and CR were calculated by integrating from near-ground to the maximum detection height, in order to make comparisons between results from these two instruments. The maximum detection height of each profile is defined according to Signal-to-Noise Ratio (SNR) with a threshold of 10. There is different observational style for these two instruments. The laser direction of the lidar is always perpendicular to the ground and points to the sky, while the observation angle of sun-photometer changes with time (especially in the morning and evening). In order to compare the data of the two observation methods, we further select the data of the sun-photometer between 10 am and 16 pm and eliminate the observation data with larger angle of the sun-photometer. To further discuss the relationship among these parameters in detail, all data points of DR and CR were divided into three intervals. The results show that the aerosol DR increases linearly with the increase of the VC, which indicates there is a good relationship between the DR and VC for aerosol loading. In addition, there is a similar relationship between the DR and ER for aerosols but with large dispersion.

It is shown that CR increases with VC, which is approximately linear. In addition, different linear DR have obvious hierarchical divisions. Moreover, DR and CR of aerosol decreases as the ER of the particle increases. When the ER of the particle is fixed, the CR increases as the DR increases. The DR increases as the CR and ER of the particle increase. In conclusion, the CR and linear DR from lidar measurements are obviously related to the aerosol VC and ER obtained by the sun-photometer. It should be noted that the correlation results may be different if the wavelength and configuration of lidar system change.

Optics EXPRESS

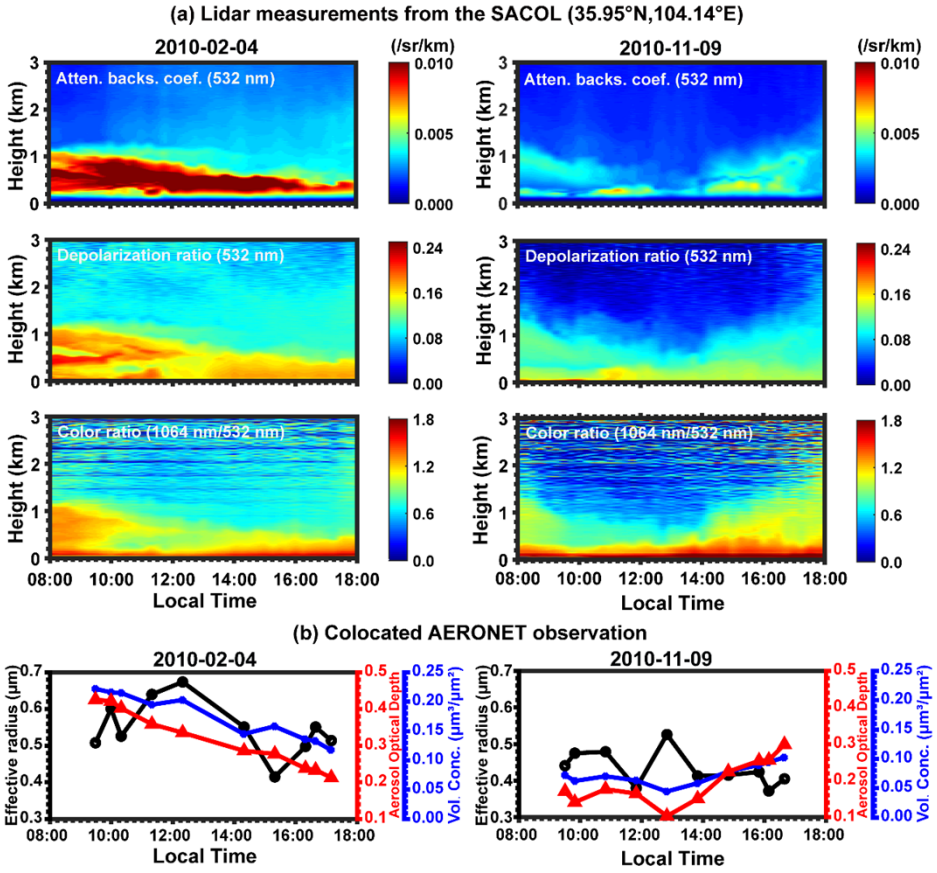

Fig. 1. (a) Vertical structure of atmospheric aerosols observed by the ground-based polarization lidar system at SACOL (35.95°N, 104.14°E) in China during a dust event (4 February) and clear day (9 November 2010); (b) Corresponding columnar microphysical properties of aerosols measured by the collocated AERONET sun-photometer (CE318).

3.1. Partial least squares regression (PLSR)

The Partial Least Squares Regression (PLSR), which was proposed by Wold [57], has developed rapidly due to combined advantages of principal component regression, canonical correlation analysis and multiple linear regression. PLSR can represent as much information as possible in the independent variable system and can explain as many changes as possible in the dependent variable system. Moreover, it can effectively solve the problem of multiple correlation between variables [58,59], which provides a way to retrieve aerosol microphysical properties from lidar measurement.

To obtain reliable aerosols VC and ER from lidar measurement, a regression model should be established in advance. The independent variables in the model are the observation results of lidar. Combined with the analysis in Fig. 1 and Fig. 2, we found that DR, CR and ABC obtained from lidar have good correlations with VC and ER, so the three key parameters are selected as the independent variables of the model. The corresponding dependent variable VC and ER can

Optics EXPRESS

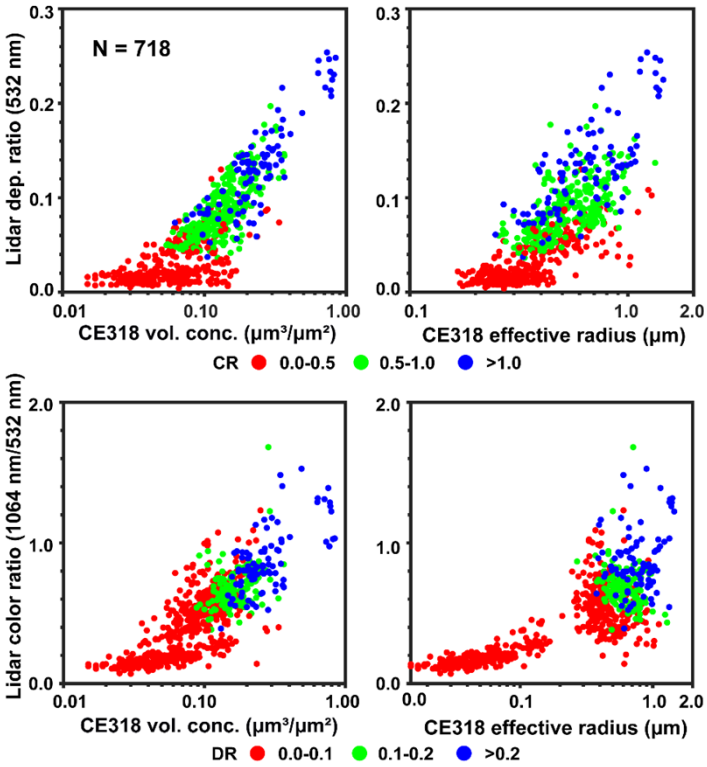

Fig. 2. Upper panel: relation between the lidar columnar DR and results from the collocated AERONET sun-photometer (CE318) at SACOL from October 2009 to March 2011 and Osaka site from 2013 to 2015. Different colors represent different ranges of the CR. Lower panel: same as the upper panel but for the columnar CR (1064 nm/532 nm). Different colors represent different ranges of the DR. The number of data points in each panel is 718

be obtained by AERONET. The PLSR model can be expressed as follow,

$$\begin{cases} VC = F_1(DR, CR, ABC) \\ ER = F_2(DR, CR, ABC) \end{cases} \tag{3}$$

F_1 and F_2 are the expected inversion formulas for VC and ER. The aerosol microphysical properties (VC and ER) can be obtained when the observation data of lidar are input.

3.2. Deep neural networks (DNN)

Compared with traditional machine learning, deep learning is able to uncover more implicit features of data, and deep neural networks (DNNs) are the frameworks of deep learning. The model is first built, then the loss function is selected to evaluate the performance of the model, and the optimizer is used to guide the loss function to continuously approach the optimum in the process of deep learning backpropagation. Generally, DNNs can be divided into input layer, hidden layer and output layer, where the hidden layer can have many layers, and all the layers are connected to each other. And the activation functions should be selected for nodes of each hidden layer. The common activation functions are ReLU, Sigmoid and so on. ReLU has simple derivation and fast convergence speed, which can effectively alleviate the gradient disappearance problem. Adamax is a variant of Adam method, which provides a simpler range for the upper

Optics EXPRESS

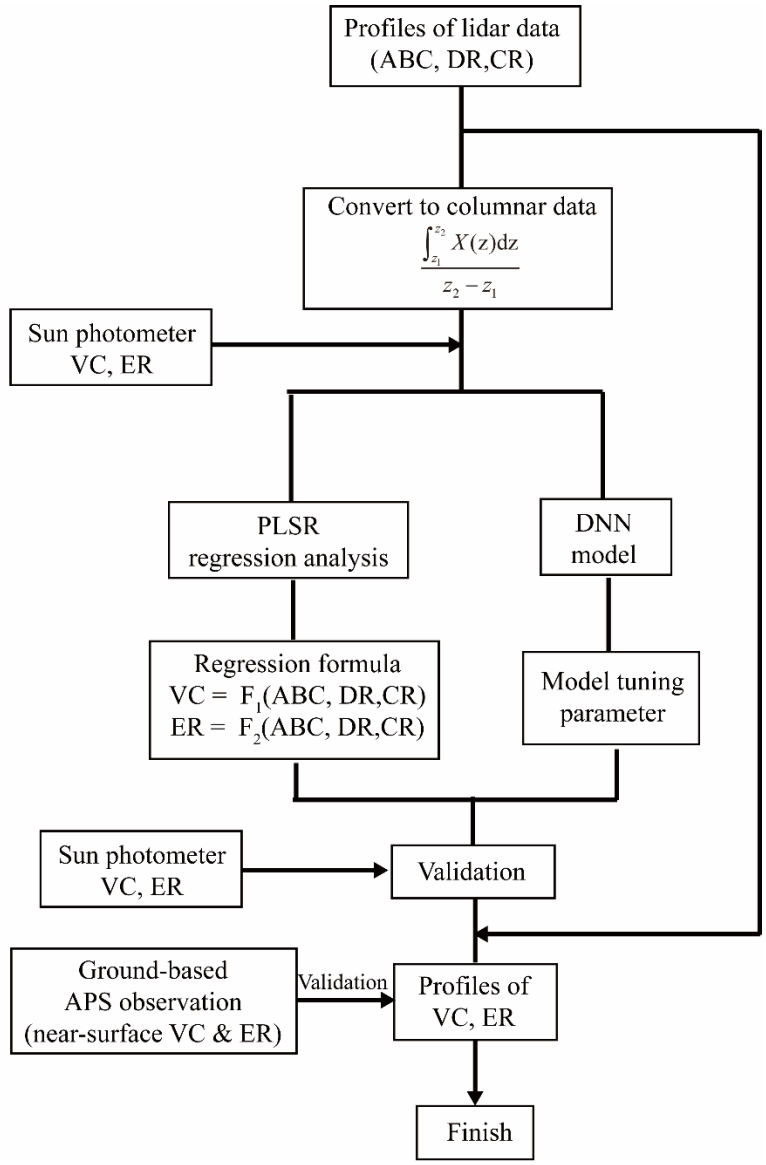

Fig. 3. A flowchart of retrieving range-resolved aerosol VC and ER from polarization lidar measurements by PLSR and DNN used in the study.

limit of learning rate, with high computational efficiency and low memory requirements. In this study, the supervised learning method is used. Similar to PLSR, an optimal model is obtained by training the existing training samples, namely the given independent variable (DR, CR and ABC) and the corresponding dependent variable (VC and ER). The model belongs to a set of functions. Then use this model to map all inputs (lidar observation data) to corresponding outputs (aerosol microphysical properties). But unlike PLSR, the formulas of the model are implicit.

The flowchart of retrieving range-resolved aerosol VC and ER from polarization lidar measurements is shown in Fig. 3. We used two methods (PLSR and DNN) for inversion. All data points at SACOL and Osaka sites are divided randomly into two groups with the same samples. Then

Optics EXPRESS

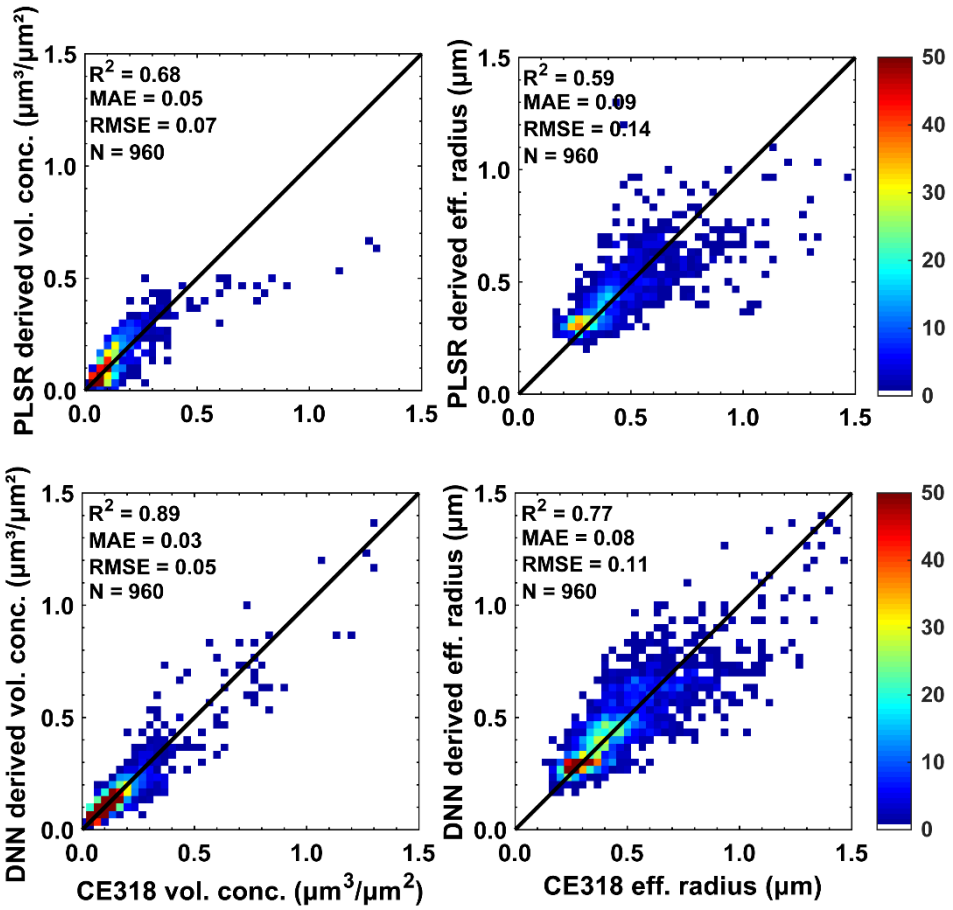

Fig. 4. Comparison of the lidar-derived columnar VC and ER with the results from the AERONET sun-photometer (CE318) observations at SACOL from October 2009 to March 2011 and in Osaka from 2013 to 2015, using the PLSR and DNN methods respectively.

group one is used to achieve the PLSR regression and DNN model using lidar and sun-photometer datasets, and group two is used to check and validation. The aerosol microphysical parameters data are taken as dependent variables, and the integration of lidar results are used as independent variables to establish the PLSR model and DNN model using group one of data points respectively. After that, columnar aerosol VC and ER were calculated using the regression formula and model tuning parameter from group two of lidar data. Consequently, lidar-derived columnar results were validated using corresponding sun-photometer data.

3.3. Validation

In this study, the two methods, PLSR and DNN are used for inversion based on lidar data. The comparisons of aerosol VC and ER between the inversion results and the observation results of AERONET are shown in Fig. 4. The first row is the inversion comparison result of PLSR, and the second line is DNN inversion comparison result.

Totally, the two inversion methods of the VC and ER at two stations are all significant with a level of 0.05. The coefficients of determination (R2) of aerosol VC and ER for both sites are 0.68 (0.89) and 0.59 (0.77) by PLSR (DNN), respectively. It is shown that the RMSE (Root Mean

Optics EXPRESS

Square Error) and MAE (Mean Absolute Error) of aerosol VC are smaller than the RMSE and MAE of ER. The inversion result of DNN is better than that of PLSR, especially in the high value of VC and ER, however, the PLSR inversion result is on the low side.

To better evaluate the retrieval results, we obtain continuous variation of lidar-based columnar aerosol VC and ER between November to December 2010 at SACOL and validated by corresponding sun-photometer results, as shown in Fig. 5. It is clearly seen that both PLSR and DNN inversion results show a good consistency with those from sun-photometer. In particular, high values of VC and ER could be characterized for December 13 and 29. Generally, the aerosol VC ranged from 0.2-0.3 $\mu m^3/\mu m^2$ at SACOL during the study period. Moreover, we also validate lidar-retrieved results between March to May, 2013 at Osaka site where exists abundant maritime aerosol, as shown in Fig. 6. For PLSR inversion method, both VC and ER are obviously underestimated. In contrast, DNN inversion results are closer to observation values. Overall, reasonable aerosol VC and ER are still obtained from polarization lidar measurements using the two retrieval methods, even though the effects are not so good as those at SACOL. The reason may be that the aerosol content in Osaka site is less than those in SACOL and the particle size is also smaller. It is worth mentioning that lidar-retrieved results can provide more information of aerosols microphysics with high temporal-resolution, even though under high cloud conditions, due to the unique advantage of active remote sensing. Therefore, lidar observational data will be useful to improve the understanding of radiative forcing estimation, and aerosol-radiation and aerosol-cloud interactions.

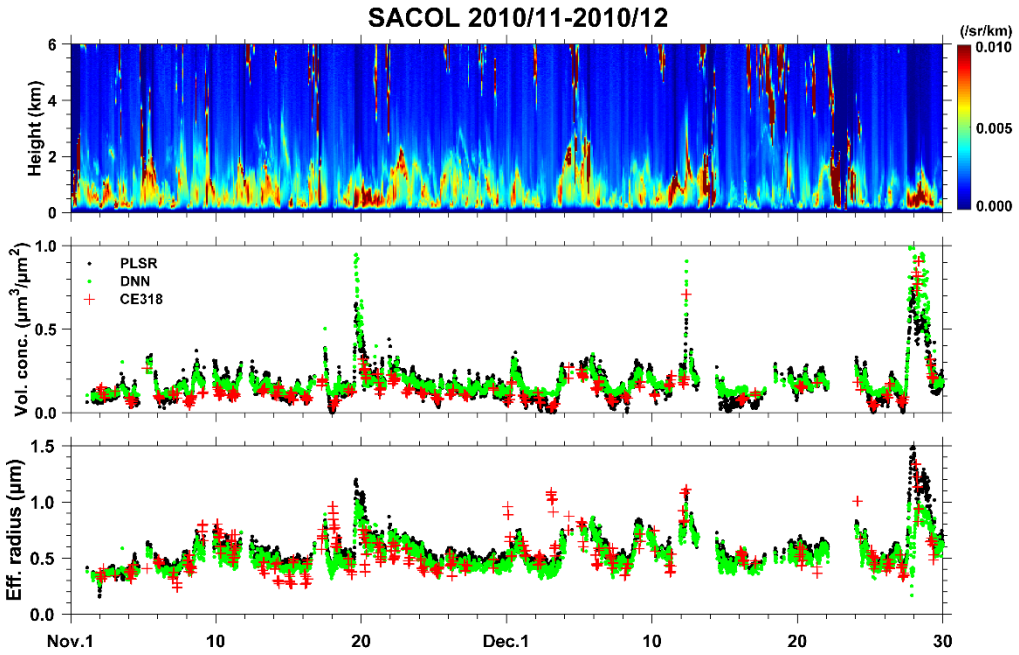

Fig. 5. Vertical structure of atmospheric aerosols and clouds from the ground-based polarization lidar measurements at SACOL from November to December 2010 and the corresponding retrieved VC and ER by PLSR (black points) and DNN methods (green points)) and AERONET sun-photometer (red crosses) observations.

Optics EXPRESS

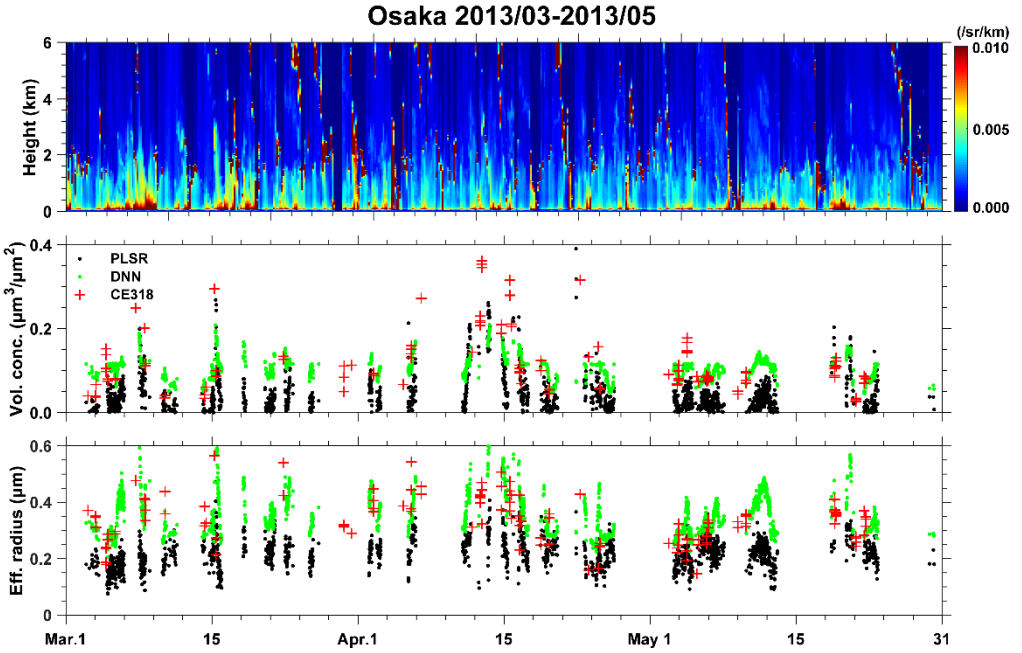

Fig. 6. Same as Fig. 5 but in Osaka from March to May, 2013.

4. Characterization of aerosol VC and ER over east Asia

The variation of aerosols microphysics is generally distinct due to its source and other related factors. To investigate the differences, monthly variations of lidar-retrieved columnar aerosol VC and ER at SACOL both for PLSR and DNN from December 2009 to November 2010 are shown in Fig. 7. The results from co-located AERONET sun-photometer observations are used for validation and comparison purpose. The results show that lidar-retrieved aerosol VC and ER have some differences from sun-photometer observations, the inversion results of PLSR and DNN are relatively close. However, the inversion results of the two methods are overestimated, especially for VC. This may be due to the lack of sun-photometer data and night observation data. However, the lidar data has high resolution and can still obtain data at night, which lead to the large differences. It is clearly seen that there is obvious seasonal variation for columnar aerosol VC and ER at SACOL. The largest VC was found in spring due to dust events that usually occurred [60,61]. It is interesting that aerosols ER in spring and winter are similar, indicating that size of air pollutants in winter are comparable to dimension of dust aerosol. The inversion and observation results of ER in summer show low values in each year, mainly because there is more precipitation in summer and washout of aerosol from the atmosphere due to more rain.

To investigate characterization of aerosol microphysics in marine environment, columnar aerosol VC and ER retrieved from lidar measurements at Osaka site is shown in Fig. 8. Obviously, the values of VC and ER of aerosols at Osaka site are much smaller than those at SACOL, illustrating that source and types of aerosols for two sites are largely different. However, seasonal variation of aerosols VC and ER at Osaka site are similar to those at SACOL. The largest aerosols VC and ER appeared in spring are consistent with previous studies [62,63]. In addition, DNN inversion results are generally higher than observations, however the PLSR results are closer to the observation results for aerosol effective radius. The inversion results of PLSR are obviously underestimated, especially for ER. In some months, the inversion results at SACOL are even

Optics EXPRESS

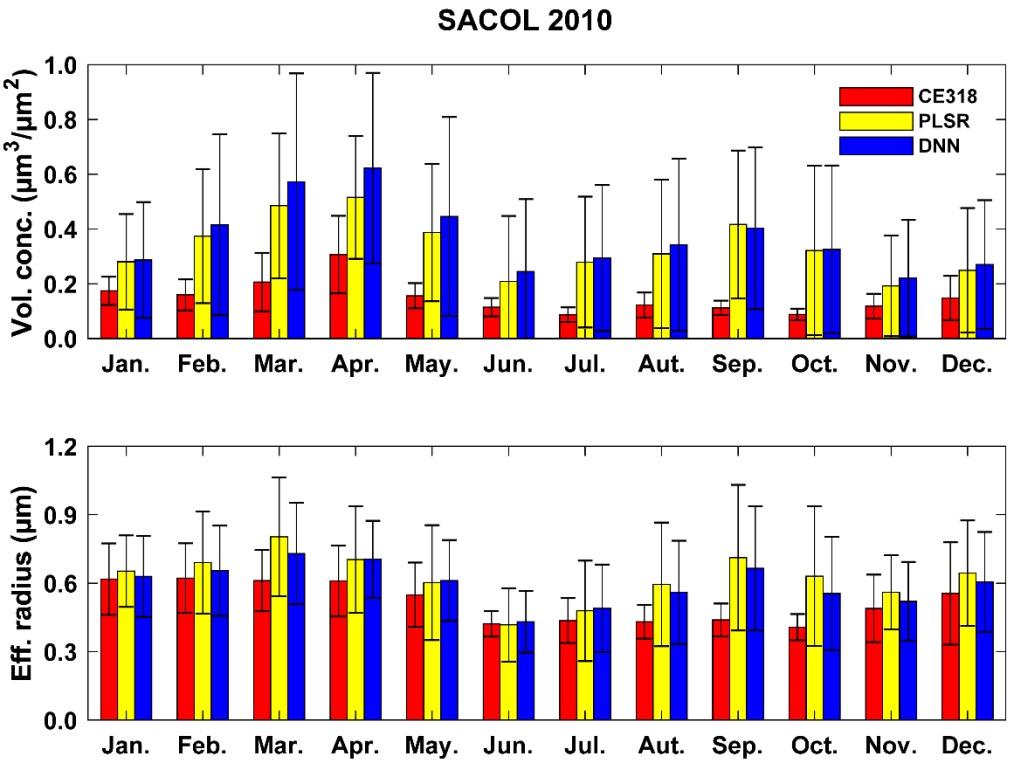

Fig. 7. Monthly variation in the VC and ER measured by CE318 (red bars) compared with those derived by PLSR (yellow bars) and DNN (blue bars) based on ground-based polarization lidar system from December 2009 to November 2010 at SACOL.

about 30% lower than the observed values, and these values may be close to Osaka Station values. Therefore, the cloud distribution has certain impacts on the inversion results in the region.

Range-resolved aerosol VC and ER is of great importantance to evaluate its radiative forcing. Here, we assess the performance of retrieval method for obtaining vertical distribution of aerosol VC and ER from lidar measurements. The aerosol VC and ER from the co-located APS observations are employed to validate the lidar-based retrieval results at the near-surface. Considering the effects of lidar blind zone, lidar-retrieved results between 200 and 350 meters above the ground level is averaged and compared with APS results in this study. Figure 9 shows near-surface aerosol VC and ER at SACOL in 2010, the first row is the comparison results of VC and ER inversion by PLSR method, and the second row is DNN. It can be seen that reliable aerosol VC and EC are obtained from lidar measurements. Aerosols VC near the earth surface is consistent with those from the APS observations. For VC, the inversion results of PLSR seem to be closer to the observation results of APS, but in fact, the distribution of corresponding points is not centralized, while the inversion result of DNN is underestimated. Objectively speaking, lidar-retrieved aerosol ER of the two methods are comparable with those from APS observations even though they are overestimated. It is concluded that height-resolved aerosol VC and ER could be reasonably retrieved from polarization measurements.

To further compare the ability of retrieval algorithm to characterize the vertical structure of aerosol VC and ER for different aerosol events, a dust case on March 9, 2010 and a haze episode on December 8, 2010 at SACOL station were selected in this study. Figure 10 shows the vertical structure of the lidar-retrieved dust aerosol VC and ER at SACOL station. The first column

Optics EXPRESS

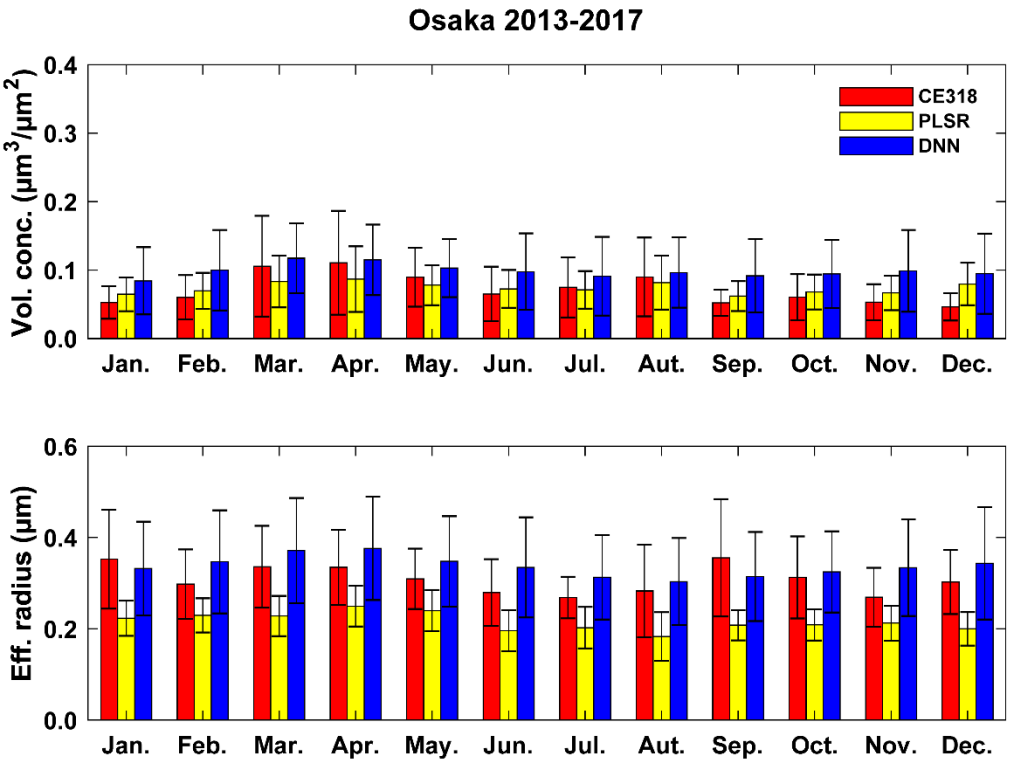

Fig. 8. Same as Fig. 7 but in Osaka from2013 to 2017.

and second column show the inversion results of PLSR and DNN, respectively, and the third column is the profiles of PLSR–derived (red line), DNN–derived (blue line) VC and ER. It can be observed that the overall trends of the two inversions are consistent, but as discussed earlier, the inversion results of DNN are slightly higher than PLSR, and the inversion results of some low values around 2 to 3 km are better. Dust layer can extend from the ground up to 3 km at midnight, however, during daytime, the deposition and spread of dust aerosols are trapped below 1 km. The dust VC and ER totally decreased with the increase of height at nighttime, but a peak occurred at about 800 m at the daytime. The vertical profiles of aerosol VC and ER are selected to show the distribution of aerosol in the vertical direction as shown in Fig. 10, in which the red real line represents the PLSR inversion results of lidar, the blue real line represents the DNN in the morning (10:00). There are some differences between the inversion results of VC and ER by the two methods. For example, for the inversion results of high aerosol content near the surface of VC, DNN is greater than PLSR, while for the inversion results of more than 1 km, PLSR is greater than DNN, while the inversion results of ER are just the opposite. During the haze episode, the aerosol VC and ER can also be characterized reliably by the two methods as shown in Fig. 11. The peaks of aerosol VC and ER always occurred at the near-surface [64]. The VC changes obviously in the vertical direction, especially under 1 km. But it fluctuates less above 1 km. The ER also presents larger values below 1 km, but decrease with height slowly and fluctuates about 0.4 μm above 1 km. For ER inversion, the results of the two methods near the ground are very close, while the results of DNN above 1 km are slightly higher than those of PLSR.

Seasonal variations of the lidar-derived VC and ER profiles at SACOL in 2010 are shown in Fig. 12. The solid line represents the PLSR inversion result, the dotted line represents the DNN inversion result, and different colors represent different seasons (blue is spring, green is

Optics EXPRESS

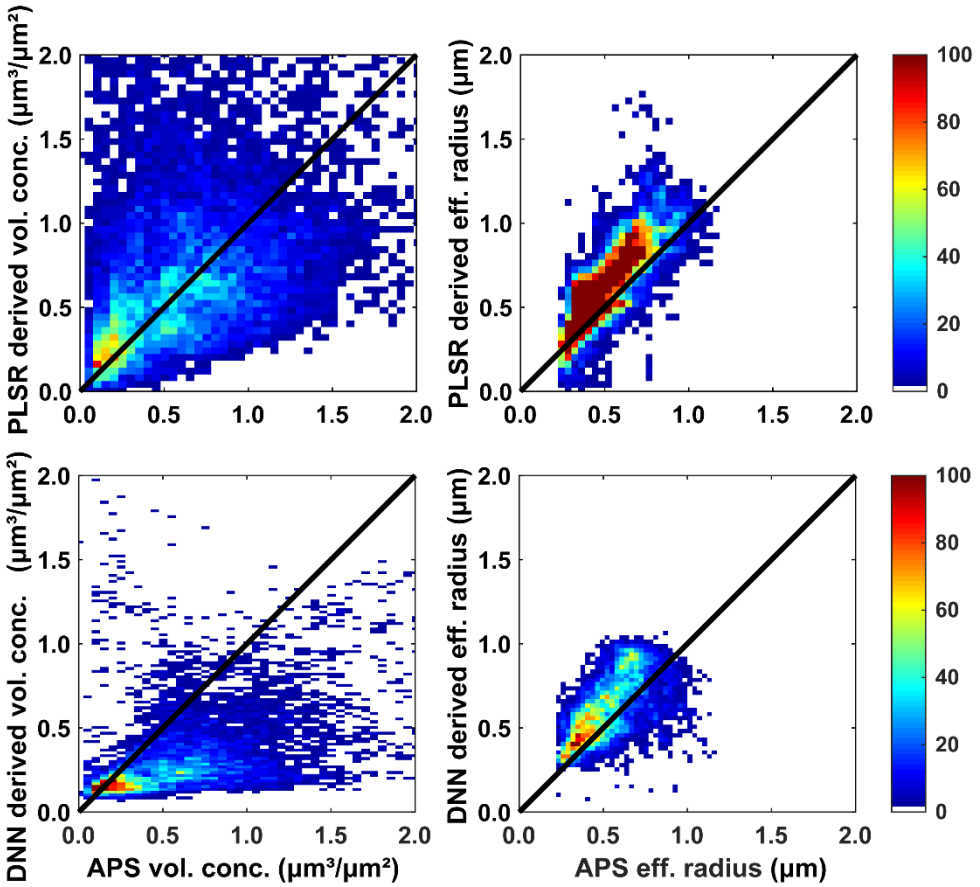

Fig. 9. Validation of range-resolved aerosol VC and ER from lidar measurements by use of collocated APS observation at SACOL in 2010.

summer, red is autumn, and black is winter). The points in the figure represent the observation results of the sun-photometer. The inversion results of VC by the two methods are relatively close, while the inversion results of ER by DNN are lower than those by PLSR. The seasonal variation characteristics of the VC and ER are the highest in spring, which are mainly due to the dry and windy spring in Western China, which is prone to dust and other events, resulting in higher aerosol concentrations [65]. The VC of aerosol in winter is slightly lower than those in spring, which is mainly due to the influence of heating and coal burning in winter, and the inversion layer often occurs over SACOL station in winter, which leads to serious pollution problems [66]. The curve of the ER of the particle with height is consistent with the change in the VC. The values of the ER in spring are higher than those in the other three seasons and are slightly lower in winter. The aerosol VC and ER in summer were the lowest ones all around the year. The columnar aerosol VC and ER observed by sun-photometer are represented by dots of different colors, and the seasonal variation trends are consistent with the profiles.

Optics EXPRESS

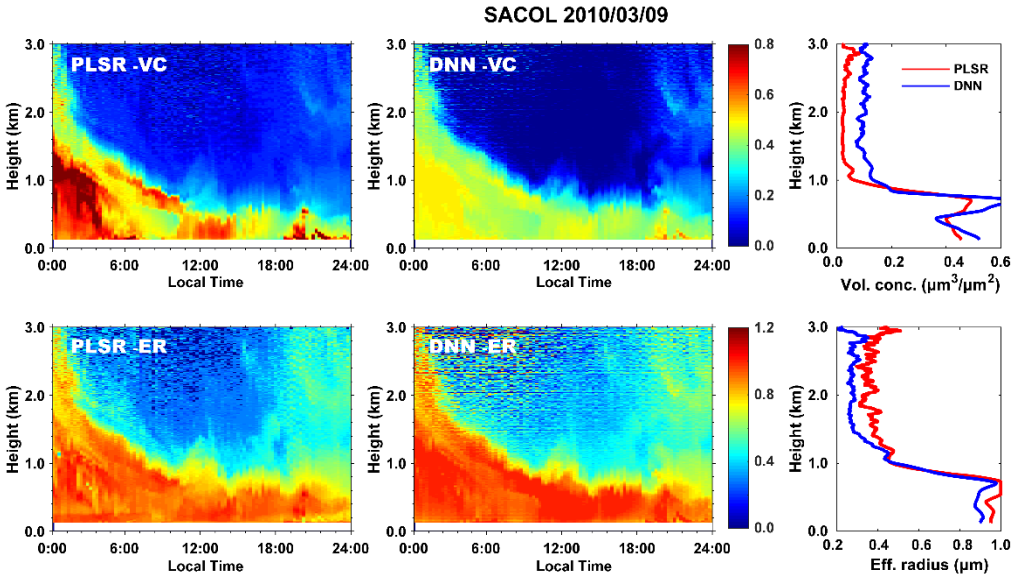

Fig. 10. Vertical structure of the lidar-derived VC and ER at SACOL during a dust event on March 9th, 2010. The first column is the inversion result of PLSR, and the second column is the inversion result of DNN and the third column is the profiles of PLSR–derived (red line), DNN–derived (blue line) VC and ER in the morning (10:00).

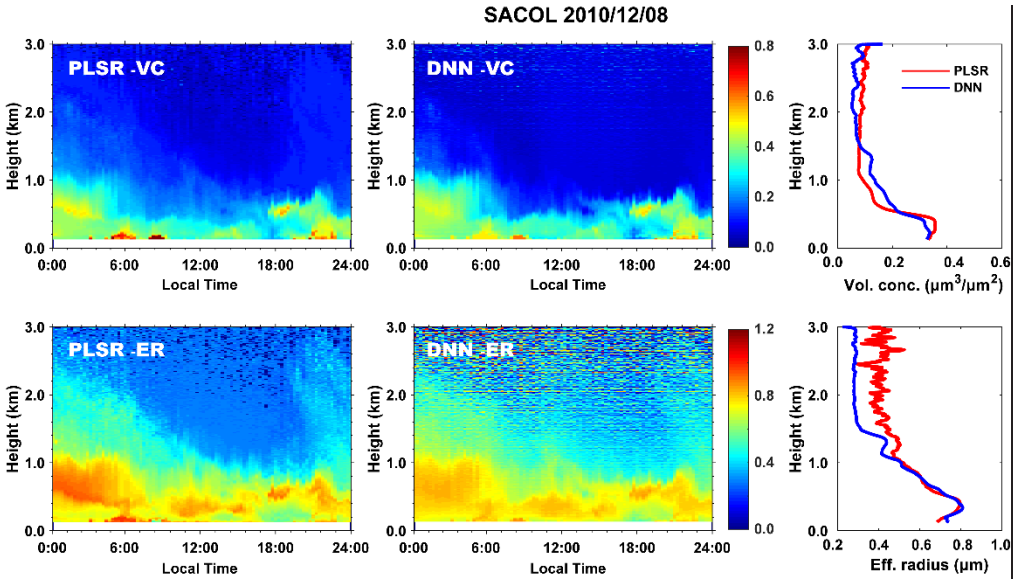

Fig. 11. Same as Fig. 10 but for a haze event on December 8th, 2010.

Optics EXPRESS

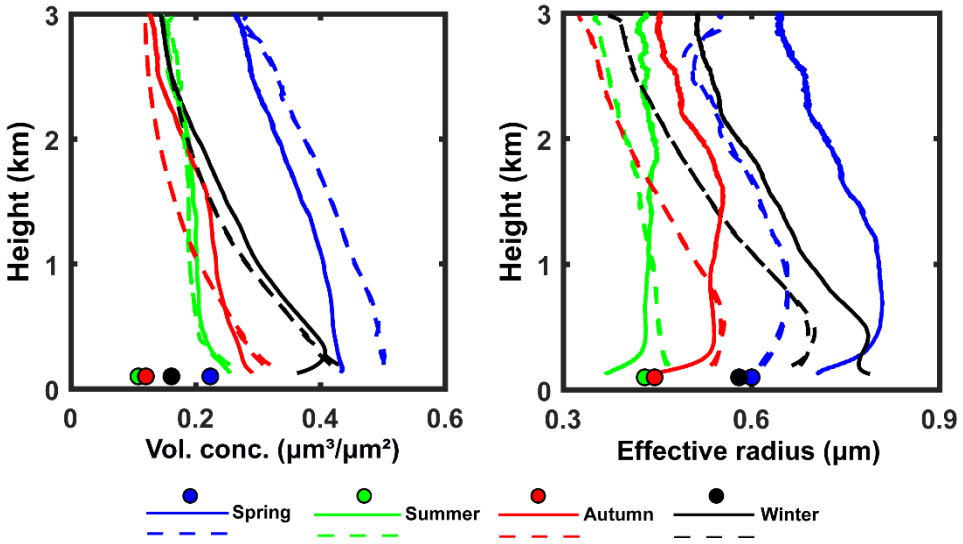

Fig. 12. Seasonal variations of lidar-derived VC and ER at SACOL in 2010. The solid line represents the PLSR inversion result, the dotted line represents the DNN inversion result, and different colors represent different seasons (blue is spring, green is summer, red is autumn, and black is winter). The points of different colors represent the observation results of the sun-photometer.

5. Conclusion

To obtain range-resolved aerosols VC and ER from remote sensing, we proposed a novel method for retrieving profiles of VC and ER of aerosols mainly by use of a ground-based Mie polarization lidar measurements in this study, based on PLSR and DNN. The inversion results of the VC and ER of two methods are significant at the 0.05 level, and the VC results are obviously better than those of the ER. The measurement coefficients of the VC and ER are 0.68 (0.89) and 0.59 (0.77) at SACOL and Osaka by PLSR (DNN) inversion. In particular, the results show that the inversion results of the two variables with long-term observation data are concentrated and reasonable. For the column integration results, the two retrieval methods are better when the VC and ER are small, but the results of DNN are better when the VC is large (more aerosols). For the profiles, the two retrieval methods perform well when the VC and ER are small, while the retrieval results of PLSR are better when the VC is large. The VC and ER from SACOL have obvious seasonal trends, and the values in spring and winter are higher than those in summer and autumn. The values are slightly lower in autumn and lowest in summer, especially in June, which is mainly due to the wet removal of aerosols due to more rainfall in summer. By comparing the average VC at heights from 200-350 m above the ground with the collocated APS observation, it is found that the ER retrieved by PLSR and DNN corresponds well, while the VC inversion result of DNN is underestimated, which may be due to different retrievals algorithms and sensor characteristics of the two instruments. The average profiles of the VC and ER of SACOL observations in each season can clearly describe the vertical characteristics of the aerosol microphysical characteristics of the site. Generally, the values of the two characteristics are the largest in spring and the smallest in summer.

Funding. Fundamental Research Funds for the Central Universities (lzujbky-2022-kb10, lzujbky-2022-kb11); 111 Project (B 13045); National Natural Science Foundation of China (41875029); the Second Tibetan Plateau Scientific Expedition and Research Program (2019QZKK0602).

Optics EXPRESS

Acknowledgment. We thank two projects, AERONET (https://aeronet.gsfc.nasa.gov/), AD-Net (https://www-lidar.nies.go.jp/AD-Net/), for providing observational data in the study.

Disclosures. The authors declare no conflicts of interest.

Data availability. Data underlying the results presented in this paper are not publicly available at this time but may be obtained from the authors upon reasonable request.

References

1. IPCC, *Climate Change 2013: The Physical Science Basis: Contribution of Working Group I to the Fifth Assessment Report of the Intergovernmental Panel on Climate Change (IPCC)*. (Cambridge University Press, 2013).
2. S. F. Abdullaev and Irina. N. Sokolik, "Main characteristics of dust storm sand their radiative impacts: With a focuson tajikistan," J. of Atmos. Sci. Res. **2**(2), 1–21 (2019).
3. Q. Fu, T. J. Thorsen, J. Su, J. M. Ge, and J. P. Huang, "Test of Mie-based single-scattering properties of non-spherical dust aerosols in radiative flux calculations," J. Quant. Spectrosc. Radiat. Transfer **110**(14-16), 1640–1653 (2009).
4. M. Hayman, S. Spuler, and B. Morley, "Polarization lidar observations of backscatter phase matrices from oriented ice crystals and rain," Opt. Express **22**(14), 16976–16990 (2014).
5. T. Wang, Y. Chen, Z. Gan, Y. Han, J. Li, and J. Huang, "Assessment of dominating aerosol properties and their long-term trend in the Pan-Third Pole region: A study with 10-year multi-sensor measurements," Atmos. Environ. **239**, 117738 (2020).
6. W. Wang, J. Huang, T. Zhou, J. Bi, L. Lin, Y. Chen, Z. Huang, and J. Su, "Estimation of radiative effect of a heavy dust storm over northwest China using Fu-Liou model and ground measurements," J. Quant. Spectrosc. Radiat. Transfer **122**, 114–126 (2013).
7. Y. Xie, Z. Li, L. Li, R. Wagener, I. Abboud, K. Li, D. Li, Y. Zhang, X. Chen, H. Xu, J. Haywood, and O. Boucher, "Aerosol optical, microphysical, chemical and radiative properties of high aerosol load cases over the Arctic based on AERONET measurements," Rev. Geophys. **8**(1), 9376 (2018).
8. A. J. Adesina, S. Piketh, R. K. Kanike, and S. Venkataraman, "Characteristics of columnar aerosol optical and microphysical properties retrieved from the sun photometer and its impact on radiative forcing over Skukuza (South Africa) during 1999-2010," Environ. Sci. Pollut. Res. **24**(19), 16160–16171 (2017).
9. J. Huang, J. Huang, X. Liu, C. Li, L. Ding, and H. Yu, "The global oxygen budget and its future projection," Sci. Bull. **63**(18), 1180–1186 (2018).
10. N. Sugimoto, I. Matsui, A. Shimizu, I. Uno, K. Asai, T. Endoh, and T. Nakajima, "Observation of dust and anthropogenic aerosol plumes in the Northwest Pacific with a two-wavelength polarization lidar on board the research vessel Mirai," Geophys. Res. Lett. **29**(19), 1–4 (2002).
11. T. Wang, Y. Han, J. Huang, M. Sun, B. Jian, Z. Huang, and H. Yan, "Climatology of dust-forced radiative heating over the tibetan plateau and its surroundings," J. Geophys. Res.: Atmos. **125**(17), 1–14 (2020).
12. R. A. Ferrare, S. H. Melfi, D. N. Whiteman, K. D. Evans, M. Poellot, and Y. J. Kaufman, "Raman lidar measurements of aerosol extinction and backscattering: 2. Derivation of aerosol real refractive index, single-scattering albedo, and humidification factor using Raman lidar and aircraft size distribution measurements," J. Geophys. Res.: Atmos. **103**(D16), 19673–19689 (1998).
13. Z. Huang, J. Huang, T. Hayasaka, S. Wang, T. Zhou, and H. Jin, "Short-cut transport path for Asian dust directly to the Arctic: A case study," Environ. Res. Lett. **10**(11), 114018 (2015).
14. Y. You, G. W. Kattawar, P. Yang, Y. X. Hu, and B. A. Baum, "Sensitivity of depolarized lidar signals to cloud and aerosol particle properties," J. Quant. Spectrosc. Radiat. Transfer **100**(1-3), 470–482 (2006).
15. Z. Huang, J. Huang, J. Bi, G. Wang, W. Wang, Q. Fu, Z. Li, S.-C. Tsay, and J. Shi, "Dust aerosol vertical structure measurements using three MPL lidars during 2008 China-U.S. joint dust field experiment," J. Geophys. Res. **115**, D00K15 (2010).
16. K. Alam, T. Trautmann, T. Blaschke, and F. Subhan, "Changes in aerosol optical properties due to dust storms in the Middle East and Southwest Asia," Remote Sens. Environ. **143**, 216–227 (2014).
17. Z. Huang, J. B. Nee, C. W. Chiang, S. Zhang, H. Jin, W. Wang, and T. Zhou, "Real-time observations of dust-cloud interactions based on polarization and Raman lidar measurements," Remote Sens. **10**(7), 1–15 (2018).
18. X. Ma, Z. Huang, S. Qi, J. Huang, S. Zhang, Q. Dong, and X. Wang, "Ten-year global particulate mass concentration derived from space-borne CALIPSO lidar observations," Sci. Total Environ. **721**, 137699 (2020).
19. T. Nishizawa, N. Sugimoto, I. Matsui, A. Shimizu, Y. Hara, U. Itsushi, K. Yasunaga, R. Kudo, and S.-W. Kim, "Ground-based network observation using Mie–Raman lidars and multi-wavelength Raman lidars and algorithm to retrieve distributions of aerosol components," J. Quant. Spectrosc. Radiat. Transfer **188**, 79–93 (2017).
20. J. W. Hair, C. A. Hostetler, A. L. Cook, D. B. Harper, R. A. Ferrare, T. L. Mack, W. Welch, L. R. Izquierdo, and F. E. Hovis, "Airborne high spectral resolution lidar for profiling aerosol optical properties," Appl. Opt. **47**(36), 6734–6753 (2008).
21. K. Kai, Y. Minamoto, K. Nakamura, M. Wang, K. Kawai, K. Ohara, J. Noda, T. Maki, E. Davaanyam, and N. Sugimoto, "Large-scale dust event in East Asia, as revealed by the Himawari-8 DUST RGB, lidar network observations, and field survey," *E3S Web of Conferences* **99**, 8–11 (2019).
22. N. Sugimoto, I. Matsui, A. Shimizu, and T. Nishizawa, "Lidar Network for Monitoring Asian Dust and Air Pollution Aerosols," in *IEEE International Geoscience & Remote Sensing Symposium* (2009).

Optics EXPRESS

23. E. Welton, L. Belcher, J. Campbell, T. Berkoff, S. Stewart, and J. Lewis, "Quality assured aerosol products from the NASA micro pulse lidar network (MPLNET)," *AGU Fall Meeting Abstracts* (2010).
24. V. Matthias, "Vertical aerosol distribution over europe: Statistical analysis of raman lidar data from 10 european aerosol research lidar network (EARLINET) stations," J. Geophys. Res. **109**(D18), D18201 (2004).
25. F. Rocadenbosch, I. Mattis, and A. Ansmann, *et al.*, "The European aerosol research lidar network (EARLINET): An overview," (2008).
26. C. David, A. Haefele, P. Keckhut, M. Marchand, J. Jumelet, T. Leblanc, C. Cenac, C. Laqui, J. Porteneuve, M. Haeffelin, Y. Courcoux, M. Snels, M. Viterbini, and M. Quatrevalet, "Evaluation of stratospheric ozone, temperature, and aerosol profiles from the LOANA lidar in Antarctica," Polar Sci. **6**(3-4), 209–225 (2012).
27. J. P. Huang, J. J. Liu, B. Chen, and S. L. Nasiri, "Detection of anthropogenic dust using CALIPSO lidar measurements," Atmos. Chem. Phys. **15**(20), 11653–11665 (2015).
28. H. Yu, M. Chin, D. M. Winker, A. H. Omar, Z. Liu, C. Kittaka, and T. Diehl, "Global view of aerosol vertical distributions from CALIPSO lidar measurements and GOCART simulations: Regional and seasonal variations," J. Geophys. Res. **115**, D00H30 (2010).
29. J. P. Vernier, L. W. Thomason, and J. Kar, "CALIPSO detection of an Asian tropopause aerosol layer," *Geophys. Res. Lett.* 38(7), n/a-n/a (2011).
30. K. Qin, L. Wu, M. S. Wong, H. Letu, M. Hu, H. Lang, S. Sheng, J. Teng, X. Xiao, and L. Yuan, "Trans-boundary aerosol transport during a winter haze episode in China revealed by ground-based Lidar and CALIPSO satellite," Atmos. Environ. **141**, 20–29 (2016).
31. J. Huang, P. Minnis, B. Chen, Z. Huang, Z. Liu, Q. Zhao, Y. Yi, and J. K. Ayers, "Long-range transport and vertical structure of Asian dust from CALIPSO and surface measurements during PACDEX," J. Geophys. Res. **113**(D23), D23212 (2008).
32. A. I. Bokoye, A. Royer, N. T. O'Neil, P. Cliche, G. Fedosejevs, P. M. Teillet, and L. J. B. McArthur, "Characterization of atmospheric aerosols across Canada from a ground-based sunphotometer network: AEROCAN," Atmos.-Ocean **39**(4), 429–456 (2001).
33. K. Schäfer, F. Molero, and A. Comerón, *et al.*, "Comparison of aerosol size distributions measured at ground level and calculated from inversion of solar radiances," (2005).
34. J. Bi, J. Huang, Z. Hu, B. N. Holben, and Z. Guo, "Investigating the aerosol optical and radiative characteristics of heavy haze episodes in Beijing during January of 2013," J. Geophys. Res.: Atmos. **119**(16), 9884–9900 (2014).
35. H. Che, X. Xia, J. Zhu, Z. Li, O. Dubovik, B. Holben, P. Goloub, H. Chen, V. Estelles, E. Cuevas-Agulló, L. Blarel, H. Wang, H. Zhao, X. Zhang, Y. Wang, J. Sun, R. Tao, X. Zhang, and G. Shi, "Column aerosol optical properties and aerosol radiative forcing during a serious haze-fog month over North China Plain in 2013 based on ground-based sunphotometer measurements," Atmos. Chem. Phys. **14**(4), 2125–2138 (2014).
36. Y. Ma, M. Zhang, S. Jin, W. Gong, N. Chen, Z. Chen, Y. Jin, and Y. Shi, "Long-term investigation of aerosol optical and radiative characteristics in a typical megacity of central china during winter haze periods," J. Geophys. Res.: Atmos. **124**(22), 12093–12106 (2019).
37. H. Di, H. Hua, Y. Cui, D. Hua, T. He, Y. Wang, and Q. Yan, "Vertical distribution of optical and microphysical properties of smog aerosols measured by multi-wavelength polarization lidar in Xi'an, China," J. Quant. Spectrosc. Radiat. Transfer **188**, 28–38 (2017).
38. Z. Huang, S. Qi, T. Zhou, Q. Dong, X. Ma, S. Zhang, J. Bi, and J. Shi, "Investigation of aerosol absorption with dual-polarization lidar observations," Opt. Express **28**(5), 7028 (2020).
39. N. Sugimoto and Z. Huang, "Lidar methods for observing mineral dust," J. Meteorol. Res. **28**(2), 173–184 (2014).
40. N. Sugimoto, Z. Huang, T. Nishizawa, I. Matsui, and B. Tatarov, "Fluorescence from atmospheric aerosols observed with a multi-channel lidar spectrometer," Opt. Express **20**(19), 20800 (2012).
41. I.-K. Song, Y.-G. Kim, S.-H. Baik, S.-K. Park, H.-K. Cha, S.-C. Choi, C.-M. Chung, and D.-H. Kim, "Measurement of aerosol parameters with altitude by using two wavelength rotational raman signals," J. Opt. Soc. Korea **14**(3), 221–227 (2010).
42. D. Althausen, D. Müller, A. Ansmann, U. Wandinger, H. Hube, E. Clauder, and S. Zörner, "Scanning 6-Wavelength 11-Channel aerosol lidar," J. Atmos. Oceanic Technol. **17**(11), 1469–1482 (2000).
43. D. Muller, F. Wagner, U. Wandinger, A. Ansmann, M. Wendisch, D. Althausen, and W. von Hoyningen-Huene, "Microphysical particle parameters from extinction and backscatter lidar data by inversion with regularization: experiment," Appl. Opt. **39**(12), 1879–1892 (2000).
44. I. Veselovskii, P. Goloub, T. Podvin, V. Bovchaliuk, Y. Derimian, P. Augustin, M. Fourmentin, D. Tanre, M. Korenskiy, D. N. Whiteman, A. Diallo, T. Ndiaye, A. Kolgotin, and O. Dubovik, "Retrieval of optical and physical properties of African dust from multiwavelength Raman lidar measurements during the SHADOW campaign in Senegal," Atmos. Chem. Phys. **16**(11), 7013–7028 (2016).
45. D. N. Whiteman, D. Pérez-Ramírez, I. Veselovskii, P. Colarco, and V. Buchard, "Retrievals of aerosol microphysics from simulations of spaceborne multiwavelength lidar measurements," J. Quant. Spectrosc. Radiat. Transfer **205**, 27–39 (2018).
46. N. Sugimoto, A. Shimizu, I. Matsui, and C. Yan, "A method for estimating mineral dust concentration in aerosol mixture using a polarization lidar," in *Conference on Lasers & Electro-Optics* (2003).

Optics EXPRESS

47. H. Che, X. Zhang, H. Chen, B. Damiri, P. Goloub, Z. Li, X. Zhang, Y. Wei, H. Zhou, F. Dong, D. Li, and T. Zhou, "Instrument calibration and aerosol optical depth validation of the China Aerosol Remote Sensing Network," J. Geophys. Res. **114**(D3), D03206 (2009).
48. B. Holben, T. Nakajima, I. Lavenu, I. Jankowiak, A. Smirnov, T. Eck, I. Slutsker, D. Tanre, J.-P. Buis, A. Setzer, E. Vermote, J. Reagan, and Y. Kaufman, "AERONET-A federated instrument network and data archive for aerosol characterization," Remote Sens. Environ. **66**(1), 1–16 (1998).
49. C. Pérez, S. Nickovic, J. M. Baldasano, M. Sicard, F. Rocadenbosch, and V. E. Cachorro, "A long Saharan dust event over the western Mediterranean: Lidar, Sun photometer observations, and regional dust modeling," J. Geophys. Res. **111**(D15), D15214 (2006).
50. S. Eck, T. F. Holben, B. N. Reid, J. S. Dubovik, O. Smirnov, A. O'Neill, N. T. Slutsker, and I. Kinne, "Wavelength dependence of the optical depth of biomass burning, urban, and desert dust aerosols," J. Geophys. Res.: Atmos. **104**(D24), 31333–31349 (1999).
51. S. Pfeifer, T. Müller, K. Weinhold, N. Zikova, S. Martins dos Santos, A. Marinoni, O. F. Bischof, C. Kykal, L. Ries, F. Meinhardt, P. Aalto, N. Mihalopoulos, and A. Wiedensohler, "Intercomparison of 15 aerodynamic particle size spectrometers (APS 3321): uncertainties in particle sizing and number size distribution," Atmos. Meas. Tech. **9**(4), 1545–1551 (2016).
52. T. M. Peters and D. Leith, "Concentration measurement and counting efficiency of the aerodynamic particle sizer 3321," J. Aerosol Sci. **34**(5), 627–634 (2003).
53. K. Willeke and P. Baron, *Aerosol measurement: Principles, techniques, and applications*, (Van Nostrand Reinhold, 2001).
54. S. Si, P. A. Jaques, Y. Zhu, M. D. Geller, and C. Sioutas, "Evaluation of the SMPS-APS system as a continuous monitor for measuring PM[sub 2.5], PM[sub 10] and coarse (PM[sub 2.5-10]) concentrations," Atmos. Environ. **36**(24), 3939–3950 (2002).
55. J. D. Yanosky, P. L. Williams, and D. L. MacIntosh, "A comparison of two direct-reading aerosol monitors with the federal reference method for PM2.5 in indoor air," Atmos. Environ. **36**(1), 107–113 (2002).
56. Z. Liu, A. Omar, M. Vaughan, J. Hair, C. Kittaka, Y. Hu, K. Powell, C. Trepte, D. Winker, C. Hostetler, R. Ferrare, and R. Pierce, "CALIPSO lidar observations of the optical properties of Saharan dust: A case study of long-range transport," J. Geophys. Res. **113**(D7), 1 (2008).
57. H. Wold, "Soft modeling by latent variables: The nonlinear iterative partial least squares approach," J. Appl. Probab. **12**(S1), 117–142 (1975).
58. L. M. Carrascal, I. Galván, and O. Gordo, "Partial least squares regression as an alternative to current regression methods used in ecology," Oikos **118**(5), 681–690 (2009).
59. R. Wehrens and B.-H. Mevik, "The pls package: Principal component and partial least squares regression in R," J. Stat. Soft. **18**(2), 1–24 (2007).
60. P. Shrestha, A. P. Barros, and A. Khlystov, "Chemical composition and aerosol size distribution of the middle mountain range in the Nepal Himalayas during the 2009 pre-monsoon season," Atmos. Chem. Phys. **10**(23), 11605–11621 (2010).
61. Q. Zhang, Z. Ning, Z. Shen, G. Li, J. Zhang, Y. Lei, H. Xu, J. Sun, L. Zhang, D. Westerdahl, N. K. Gali, and X. Gong, "Variations of aerosol size distribution, chemical composition and optical properties from roadside to ambient environment: A case study in Hong Kong, China," Atmos. Environ. **166**, 234–243 (2017).
62. I. Sano, S. Mukai, M. Nakata, N. Sugimoto, and B. N. Holben, "Local distribution of PM2.5 concentration over Osaka based on space and ground measurements," Proc of SPIE **8534**, 85340C (2012).
63. M. Nakata, I. Sano, S. Mukai, and B. N. Holben, "Spatial and temporal variations of atmospheric aerosol in Osaka," Atmosphere **4**(2), 157–168 (2013).
64. I. Veselovskii, D. N. Whiteman, M. Korenskiy, A. Kolgotin, O. Dubovik, D. Perez-Ramirez, and A. Suvorina, "Retrieval of spatio-temporal distributions of particle parameters from multiwavelength lidar measurements using the linear estimation technique and comparison with AERONET," Atmos. Meas. Tech. **6**(10), 2671–2682 (2013).
65. J. Huang, W. Zhang, J. Zuo, J. Bi, J. Shi, X. Wang, Z. Chang, Z. Huang, S. Yang, B. Zhang, G. Wang, G. Feng, J. Yuan, L. Zhang, H. Zuo, S. Wang, C. Fu, and C. Jifan, "An overview of the semi-arid climate and environment research observatory over the loess plateau," Adv. Atmos. Sci. **25**(6), 906–921 (2008).
66. J. Bi, J. Huang, B. Holben, and G. Zhang, "Comparison of key absorption and optical properties between pure and transported anthropogenic dust over East and Central Asia," Atmos. Chem. Phys. **16**(24), 15501–15516 (2016).